Wave Motion 48 (2011) 392–400

Contents lists available at ScienceDirect

Wave Motion

journal homepage: www.elsevier.com/locate/wavemoti

Off-axial acoustic scattering of a high-order Bessel vortex beam by a rigid sphere

F.G. Mitri [a,*], G.T. Silva [b]

[a] Los Alamos National Laboratory, MPA-11, Sensors & Electrochemical Devices, Acoustics & Sensors Technology Team, MS D429, Los Alamos, NM 87545, USA
[b] Instituto de Física, Universidade Federal de Alagoas, Maceió, Alagoas, 57072-970, Brazil

ARTICLE INFO

Article history:
Received 8 October 2010
Received in revised form 25 January 2011
Accepted 7 February 2011
Available online 16 February 2011

Keywords:
Acoustic scattering
Bessel vortex beam
Off-axial scattering
Rigid sphere

ABSTRACT

In this paper, the off-axial acoustic scattering of a high-order Bessel vortex beam by a rigid immovable (fixed) sphere is investigated. It is shown here that shifting the sphere *off* the axis of wave propagation induces a dependence of the scattering on the azimuthal angle. Theoretical expressions for the incident and scattered field from a rigid immovable sphere are derived. The near- and far-field acoustic scattering fields are expressed using partial wave series involving the spherical harmonics, the scattering coefficients of the sphere, the half-conical angle of the wave number components of the beam, its order and the beam-shape coefficients. The scattering coefficients of the sphere and the 3D scattering directivity plots in the near- and far-field regions are evaluated using a numerical integration procedure. The calculations indicate that the scattering directivity patterns near the sphere and in the far-field are strongly dependent upon the position of the sphere facing the incident high-order Bessel vortex beam.

1. Introduction

Wave scattering from regularly- and irregularly-shaped objects occurs in nature, in which some forms of radiation, such as light, sound, or even gravitational waves deviate from their incident trajectory to form a well-defined scattering pattern in space [1].

As an example in the field of acoustics, this topic is investigated extensively in underwater applications [2–5] with the aim of indentifying targets from their sonar echoes. In most of these important investigations, scattering from plane (axisymmetric) waves is only considered [6]. Therefore, the acoustic scattering is not dependent on the incident beam's parameters. Nevertheless, when the incident beam is in the form of a Gaussian focused (finite) beam [7–10], a zero-order [11], or a high-order Bessel vortex beam [12–14], the scattered field strongly depends on the beam's parameters, such as the beam's focus, and the half-cone angle of incidence. In those studies, however, the *axial* acoustic scattering is only investigated such that the target is *centered* along the axis of propagation of the incident waves.

It is nonetheless recognized that a *complete* solution of the problem requires solving for *both* the on- and off-axial acoustic scattering. Despite the significant scientific reports investigating the *axial* acoustic scattering by a sphere, the lack of such a solution provides us with the impetus to tackle this problem. A theoretical derivation is established here to study these effects and determine the acoustic pressure distribution of a mono-frequency high-order Bessel vortex beam incident upon a rigid sphere. Such beams have attracted significant attention and considerable investigations in optics and acoustics applications because they belong to the family of non-diffracting beams that do not spread while propagating in space (See section II.A in [15] for a detailed discussion). Furthermore, they are self-healing; if part of the beam is obstructed or distorted, the beam reconstructs itself after a

* Corresponding author.
E-mail address: mitri@lanl.gov (F.G. Mitri).

0165-2125/$ – see front matter © 2011 Elsevier B.V. All rights reserved.
doi:10.1016/j.wavemoti.2011.02.001

characteristic propagation distance [16]. Thus, such beams have provided an attractive alternative to using standard Gaussian beams in various applications [17–20].

In this paper, a general spherical coordinate separation-of-variables solution for the incident and scattered acoustic pressures, as well as numerical simulations are presented for the determination of the scattered acoustic pressure distribution both near the surface of a rigid immovable sphere and in the far-field region. The incident field is composed of a high-order Bessel vortex beam of *arbitrary* character. Calculations for the rigid sphere in non-viscous water demonstrating the effects of shifting the sphere *off* the beam's axis are presented. Some aspects and properties of the near- and far-field acoustic scattering are discussed in full detail. An understanding of the scattering properties is central for analyzing the acoustic radiation forces [21–26] and torques on spheres and may be helpful in the development of an "acoustic blender" [27] and tweezers for rotating and manipulating small objects.

2. Theory and analysis

Consider an acoustical wave field emerging from an arbitrarily shaped aperture propagating in an ideal fluid incident upon a rigid sphere and described by its complex pressure $P^{(inc.)}$ that is a solution of the Helmholtz wave equation,

$$\left(\nabla^2 + k^2\right)P^{(inc.)} = 0, \tag{1}$$

where k is the wave number.

In a system of spherical coordinates (r, θ, ϕ) with its origin chosen at the center of the sphere (See Fig. 1), the most general separation of variables solution of the Helmholtz Eq. (1) is given by

$$P^{(inc.)}(r,\theta,\phi) = P_0 \sum_{p=0}^{\infty} \sum_{q=-p}^{p} \left[a_{pq}(ka) j_p(kr) + b_{pq}(ka) y_p(kr)\right] Y_p^q(\theta,\phi), \tag{2}$$

where P_0 is the pressure amplitude, $a_{pq}(ka)$ and $b_{pq}(ka)$ are arbitrary beam-shape coefficients, $j_p(.)$ and $y_p(.)$ are the spherical Bessel function of the first and second kind, respectively, and $Y_p^q(.)$ are the qth-order spherical harmonics of pth-degree. The factor $\exp(-i\omega t)$ is suppressed from Eq. (2) since the space-dependent pressure is only concerned. It is important to note here that Eq. (2) represents a general solution of Eq. (1), however it requires specific boundary conditions to be used in a real physical system. In the description of acoustical (or optical) high-order Bessel (vortex) beams, which describe a wave-field that is physically finite at the origin ($r=0$), the parameter $b_{pq}(ka)=0$, and the spherical Bessel functions of the second kind $y_p(.)$ may be excluded since they represent a singularity at the origin.

Without loss of generality, the incident pressure field is therefore rewritten as

$$P^{(inc.)}(r,\theta,\phi) = P_0 \sum_{p=0}^{\infty} \sum_{q=-p}^{p} a_{pq}(ka) j_p(kr) Y_p^q(\theta,\phi). \tag{3}$$

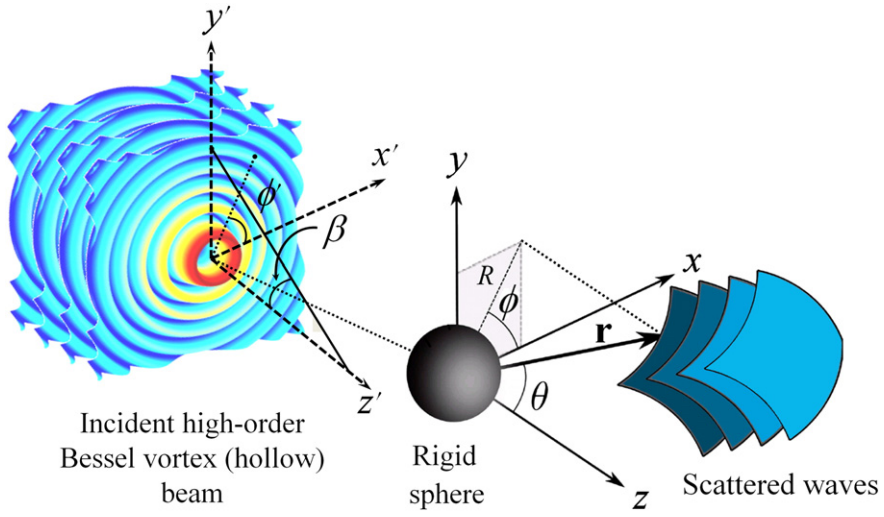

Fig. 1. Geometry of the problem. The primed coordinate system has its origin at the center of the beam, while the unprimed coordinate system is referenced to the sphere center.

Consider a spherical target immersed in a non-viscous fluid, and placed arbitrarily in the field of the incident pressure field as given by Eq. (3). The presence of the spherical target in the waves' path causes the incident field to scatter. The scattered field is represented by

$$P^{(sc.)}(r,\theta,\phi) = P_0 \sum_{p=0}^{\infty} \sum_{q=-p}^{p} a_{pq}(ka) S_p(ka) h_p^{(1)}(kr) Y_p^q(\theta,\phi), \tag{4}$$

where $h_p^{(1)}(.)$ are the spherical Hankel functions of the first kind, and $S_p(ka)$ are the scattering partial wave coefficients of the sphere determined by applying appropriate boundary conditions at the interface fluid-structure, with the assumption that the fluid is ideal. These functions generally depend on the sphere's material parameters such as the longitudinal sound speed c_L, the shear or transverse sound speed c_T, and the mass densities of both the fluid ρ_f and the sphere ρ_s. For a rigid immovable sphere, these coefficients are determined using the solution that satisfies the boundary condition of the vanishing of the particle velocity at the boundary $r=a$ such that,

$$S_p(ka) = -j_p'(ka) / h_p^{(1)'}(ka), \tag{5}$$

where a is the sphere's radius.

To determine the beam-shape coefficients $a_{pq}(ka)$, the analogy with the representation of the electric field [i.e. (29) in [28]] is used to express the incident acoustic pressure at the surface of the sphere (i.e. $r=a$) as

$$P^{(inc.)}(r=a,\theta,\phi) = P_0 \sum_{p=0}^{\infty} \sum_{q=-p}^{p} a_{pq}(ka) j_p(kr) Y_p^q(\theta,\phi). \tag{6}$$

The coefficients $a_{pq}(ka)$ are then determined by applying the orthogonality condition of the spherical harmonics $\int_{\phi=0}^{2\pi}\int_{\theta=0}^{\pi} Y_p^q(\theta,\phi) Y_{p'}^{q'*}(\theta,\phi) d\Omega = \delta_{pp'}\delta_{qq'}$, where $\delta_{ij} = \begin{cases} 1, & if\ i=j, \\ 0, & if\ i\neq j, \end{cases}$ is the Kronecker's delta function and $d\Omega = \sin\theta d\theta d\phi$. Accordingly, these coefficients are expressed as

$$a_{pq}(ka) = \frac{1}{j_p(ka) P_0} \int_{\phi=0}^{2\pi} \left[\int_{\theta=0}^{\pi} P^{(inc.)}(r=a,\theta,\phi) Y_p^{q^*}(\theta,\phi) sin\theta d\theta \right] d\phi, \tag{7}$$

where the superscript "*" denotes a complex conjugate.

After determining the beam-shape coefficients $a_{pq}(ka)$, the scattered pressure field can be evaluated after substituting Eq. (7) into Eq. (4) using Eq. (5).

For the case of a generalized Bessel vortex beam of order m, the incident pressure field, that is a proper solution of the homogeneous Helmholtz Eq. (1), is expressed in a coordinate system (x', y', z') with its origin chosen at the center of the beam (Fig. 1), where $\phi' = \tan^{-1}(y'/x')$, and $R' = \sqrt{(x'^2 + y'^2)}$, as

$$P^{(inc.)} = P_0 e^{ik_z z'} J_m(k_r R') e^{im\phi'}, \tag{8}$$

where $J_m(.)$ is the cylindrical Bessel function of the first kind of positive order m (that can be also negative, however this case is excluded here), $k_z = k\cos\beta$ and $k_r = k\sin\beta$ are the axial and radial wave-numbers, β is the half-cone angle formed by the wave-number k relative the axis of wave propagation, and ϕ', and z' are the azimuthal and axial components, respectively.

In a system of spherical coordinates with its origin chosen at the center of the sphere, it has been shown in a previous work [12] that the incident pressure of a high-order Bessel (vortex) beam coinciding with the axis of wave propagation, and represented by a cylindrical wave function given by Eq. (8), is expressed as a closed-form mathematical equation [12,14],

$$\begin{aligned} P^{(inc.)}(r,\theta,\phi) &= P_0 e^{ik_z r cos\theta} J_m(k_r r sin\theta) e^{im\phi} = P_0 e^{ikrcos\beta cos\theta} J_m(kr\sin\beta\sin\theta) e^{im\phi}, \\ &= P_0 \sum_{n=m}^{\infty} \frac{(n-m)!}{(n+m)!} (2n+1) i^{(n-m)} j_n(kr) P_n^m(cos\theta) P_n^m(cos\beta) e^{im\phi}, \end{aligned} \tag{9}$$

where $P_n^m(.)$ are the associated Legendre functions of order m and degree n.

Rewriting Eq. (9) as a double-summation series as,

$$\begin{aligned} P^{(inc.)} &= P_0 \sum_{n=m}^{\infty} \frac{(n-m)!}{(n+m)!} (2n+1) i^{(n-m)} j_n(kr) P_n^m(cos\theta) P_n^m(cos\beta) e^{im\phi}, \\ &= P_0 \sum_{n=0}^{\infty} \sum_{\ell=-n}^{n} \frac{(n-\ell)!}{(n+\ell)!} \delta_{\ell m} H(n-m) (2n+1) i^{(n-\ell)} j_n(kr) P_n^{\ell}(cos\theta) P_n^{\ell}(cos\beta) e^{i\ell\phi}, \end{aligned} \tag{10}$$

where the parameter ℓ is a dummy summation index, the factor $H(n-m) = \begin{cases} 1, & if\ (n-m)\geq 0, \\ 0, & if\ (n-m)<0, \end{cases}$ is the discrete Heaviside step function, and comparing Eq. (10) with Eq. (3) using the well-known identity for the spherical harmonics,

$$Y_p^q(\theta,\phi) = \sqrt{\frac{(2p+1)}{4\pi}\frac{(p-q)!}{(p+q)!}}P_p^q(cos\theta)e^{iq\phi}, \tag{11}$$

leads to the determination of the beam-shape coefficients for the *on-axis scattering* as follows,

$$a_{pq}|_{on-axis} = a_{nm}|_{on-axis} = i^{(n-m)}P_n^m(cos\beta)\sqrt{4\pi(2n+1)\frac{(n-m)!}{(n+m)!}}H(n-m). \tag{12}$$

It is common to investigate the acoustic scattering in the far-field region. Therefore, in the far-field region ($kr\to\infty$), the steady-state (time-independent) scattered pressure from a sphere [29,30] using Eq. (4) is expressed as

$$P^{(sc.)}(r,\theta,\phi)\underset{kr\to\infty}{=} P_0\frac{a}{2r}f_\infty(ka,\theta,\beta,\phi)e^{ikr}, \tag{13}$$

where the spherical Hankel function of the first kind reduces to the following asymptotic approximation; $h_p^{(1)}(kr)\xrightarrow[kr\to\infty]{}\frac{1}{i^{(p+1)}kr}e^{ikr}$.

The (complex) form function for a sphere $f_\infty(ka,\theta,\beta,\phi)$, is therefore defined by the exact partial wave series as

$$f_\infty(ka,\theta,\beta,\phi) = \frac{2}{ika}\sum_{p=0}^{\infty}\sum_{q=-p}^{p}a_{pq}(ka)i^{(-p)}S_p(ka)Y_p^q(\theta,\phi). \tag{14}$$

3. Numerical results and discussion

To explore the theory and illustrate the nature and the behavior of the solution related to the on- and off-axis far-field acoustic scattering by a rigid sphere, a computer program is developed using MATLAB® software package. Accurate computation of the spherical Bessel and spherical Hankel functions and their derivatives is achieved using modified versions of the specialized math functions "besselj", "bessely" and "besselh" within the software package. The computations are performed on an Intel(R) Core (TM)2 Quad CPU Q9650 @ 3.00 GHz, 3.25 GB of RAM personal computer with a truncation constant $p_{max}>>ka$ and corresponding to the biggest order included to ensure proper convergence of the series. Calculation of the beam-shape coefficients requires determining the surface integral in Eq. (7). The numerical procedure consists of sampling the integrand (i.e. pressure) over the sphere's surface. The integral is then evaluated by quadrature based on a Riemann sum in the MATLAB® software package. It is important to emphasize that dense grids are required in both the θ and ϕ directions to obtain proper convergence of the numerical integrations.

The main interest is to evaluate the magnitude of the on- and off-axis acoustic scattering by a rigid sphere in the near-field by substituting Eq. (8) into Eq. (7) and then plugging the result into Eq. (4), as well as the far-field through the form function given by Eq. (14) using Eqs. (7) and (8). The beam-shape coefficients $a_{pq}(ka)$ are evaluated numerically by discretizing the integral in

Table 1
The zeros of the spherical Bessel function of the first kind computed using the "fzero" function in MATLAB® software package in the range $0\leq x\leq 50$ (The table lists the values of the parameter x for which $j_p(x)=0$).

ℓ	$j_0(x)$	$j_1(x)$	$j_2(x)$	$j_3(x)$	$j_4(x)$	$j_5(x)$	$j_6(x)$	$j_7(x)$	$j_8(x)$	$j_9(x)$	$j_{10}(x)$
1	π	0	0	0	0	0	0	0	0	0	0
2	2π	4.49341	5.76346	6.98793	8.18256	9.35581	10.5128	11.657	12.7908	13.9158	15.0335
3	3π	7.72525	9.09501	10.4171	11.7049	12.9665	14.2074	15.4313	16.641	17.8386	19.0259
4	4π	10.9041	12.3229	13.698	15.0397	16.3547	17.648	18.923	20.1825	21.4285	22.6627
5	5π	14.0662	15.5146	16.9236	18.3013	19.6532	20.9835	22.2953	23.5913	24.8732	26.1428
6	6π	17.2208	18.689	20.1218	21.5254	22.9046	24.2628	25.6029	26.927	28.2371	29.5346
7	7π	20.3713	21.8539	23.3042	24.7276	26.1278	27.5079	28.8704	30.2173	31.5502	32.8705
8	8π	23.5195	25.0128	26.4768	27.9156	29.3326	30.7304	32.1112	33.4768	34.8287	36.1682
9	9π	26.6661	28.1678	29.6426	31.0939	32.5247	33.9371	35.3332	36.7145	38.0825	39.4382
10	10π	29.8116	31.3201	32.8037	34.2654	35.7076	37.1323	38.5414	39.9361	41.3179	42.6877
11	11π	32.9564	34.4705	35.9614	37.4317	38.8836	40.3189	41.7391	43.1454	44.5391	45.9212
12	12π	36.1006	37.6194	39.1165	40.5942	42.0544	43.4988	44.9286	46.3451	47.7493	49.1422
13	13π	39.2444	40.7671	42.2695	43.7536	45.2211	46.6733	48.1117	49.5371		
14	14π	42.3879	43.914	45.421	46.9106	48.3844	49.8437				
15	15π	45.5311	47.0601	48.5711							
16		48.6741									

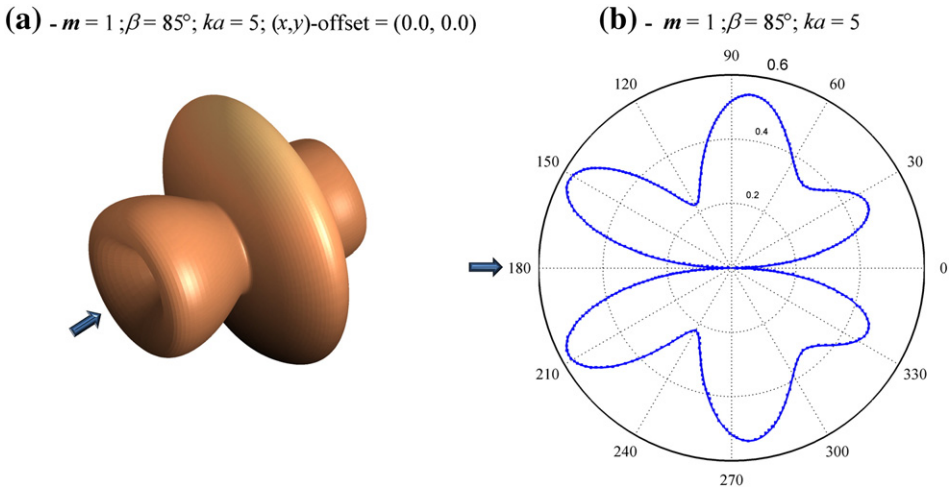

Fig. 2. (a) shows the 3D directivity pattern for the *axial* far-field scattering obtained using the numerical integration, whereas (b) shows a comparison between the numerical (dotted line) and the closed-form analytical (solid line) solutions corresponding to the polar 2D plots. The acoustical waves form a first-order Bessel vortex beam (i.e. $m=1$), with a size parameter $ka=5$ and a half-cone $\beta=85°$. The arrows on the left-hand side of (a) and (b) indicate the direction of the incident waves. Perfect agreement is noticed.

Eq. (7). Its inspection shows that the denominator involves the spherical Bessel function of the first kind $j_p(ka)$. A particular care needs then to be paid to the choice of ka so as to avoid the zeros of $j_p(ka)$, hence, the resulting indeterminacies that may appear while evaluating the integral. Appropriate selection of ka requires excluding those to corresponding zeros of $j_p(ka)$ that are listed in Table 1 for convenience.

Initially, a test is performed to verify the accuracy and correctness of the numerical findings. The test requires computing and comparing the *on-axis* scattering results of the present theory with the ones obtained from the *axial* scattering theory using a closed-form solution previously developed and published in [12,14]. Fig. 2-(a),(b) shows a comparison between the directivity pattern result for the *axial* far-field scattering obtained by using the numerical integration (i.e. "(x,y)-offset = (0,0)" corresponds to a sphere centered on the beam's axis, and the closed-form solution. For this test example, the acoustical waves are selected to form a first-order Bessel vortex beam (i.e. $m=1$), with a size parameter $ka=5$ and a half-cone $\beta=85°$. The arrows on the left-hand side of (a) and (b) indicate the direction of the incident waves. As observed from this figure, excellent agreement is obtained

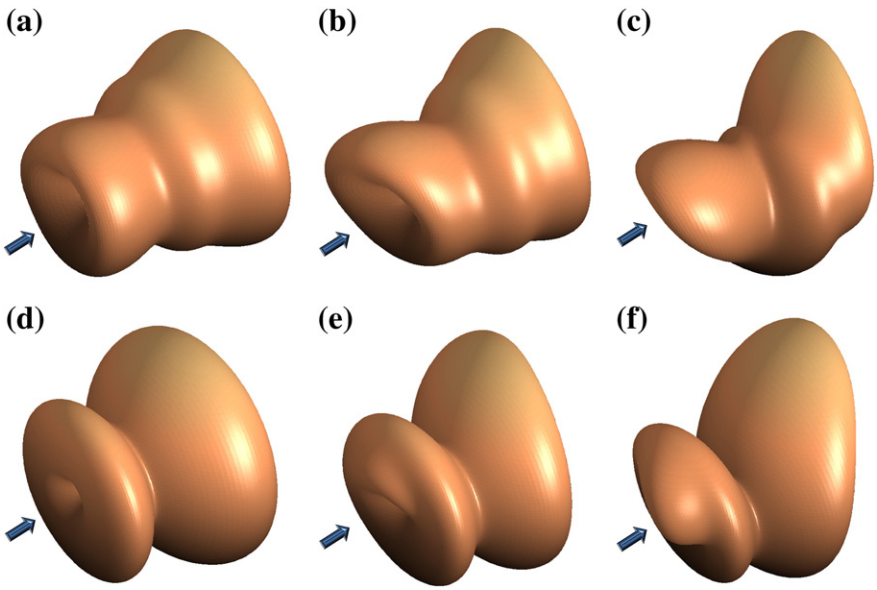

Fig. 3. Comparison between the 3D directivity plots in the near-field (i.e. $r=1.2a$) (first row, (a)–(c)) and the far-field (second row, (d)–(f)) for a rigid sphere in the field of a first-order ($m=1$) Bessel vortex beam. The half-cone angle is $\beta=45°$ and $ka=5$. In (a),(d), the sphere is centered on the beam's axis. In (b),(e), the sphere is shifted only in the x direction such that the offset is (x,y)-offset = $(0.1\lambda/2a;0)$. In (c),(f), the sphere is shifted in both x and y directions such that the offset is (x,y)-offset = $(0.1\lambda/2a;\ 0.2\lambda/a)$. The arrows on the left-hand side indicate the direction of the incident waves.

between the two methods. Additional examples and further tests (not shown here) with higher-order ($m>1$) Bessel vortex beams for different size parameters (excluded from Table 1) and half-cone values have been performed and provided excellent matching between the two methods.

To illustrate the effect of shifting the sphere *off* the axis of the beam, the acoustic scattering of a first-order ($m=1$) Bessel vortex beam with $\beta=45^\circ$ at $ka=5$ is investigated. The 3D directivity plots are displayed in Fig. 3. The top row (i.e. Fig. 2-(a)–(c)) displays the scattering in the near-field for $r=1.2a$ for three different cases: in (a) the sphere is centered on the beam's axis such that the (x,y)-offset is zero. In (b), the sphere is shifted only in the x direction such that the offset is (x,y)-offset $=(0.1\lambda/2a;0)$. In (c), the sphere is shifted in both x and y directions such that the offset is (x,y)-offset $=(0.1\lambda/2a;\ 0.2\lambda/a)$. The arrows on the left-hand side indicate the direction of the incident waves. The bottom row in Fig. 3-(d)–(f) shows the 3D directivity plots in the far-field without (Fig. 3-(d)) and with (Fig. 3-(e),(f)) displacement offsets taking the same values as in (b) and (c) respectively. It is obvious that the on-axis scattering displayed in (a),(d) shows perfectly symmetric directivity patterns and is significantly different from the off-axial scattering as shown in (b),(c),(e) and (f). Moreover, the characteristic property of the first-order Bessel vortex beam related to the pressure null at the center of the (hollow) beam is strongly manifested in the *axial* scattering such that the forward and backward acoustic scattering from the sphere (along the axis) vanish. This is somewhat predicted from Eq. (10) because of the dependence on the associated Legendre functions $P_n^m(\cos\theta)$ that vanish for $\theta=0^\circ$ (i.e. forward direction) and $\theta=180^\circ$ (backward direction). This is a property of the high-order Bessel vortex beam (i.e. $m>0$). However, as the offset increases, the scattering pattern loses symmetry and takes particular directivity patterns determined by the amount of the offset (See also Animated supplementary file 1). In the supplementary animation file 1, the 3D scattering directivity patterns have been calculated for a sphere that is shifted off-axially in the bandwidth $0\le x\le 1.2127$ in incremental steps of $\delta x=\lambda/200a=0.0063$.

It is obvious from Fig. 3 that near- and far-field scattering directivity plots are not alike. Additional on- and off-axis calculations (not shown here) for a first-order Bessel vortex beam are performed in the near-field while increasing the distance r from the center of the sphere in increments of 0.1. It is verified that when r largely exceeds a (i.e. $r>5a$ and beyond, i.e. $r\to\infty$), the near-field scattering directivity plots closely approach the far-field scattering patterns.

Further calculations for the far-field acoustic scattering of a first-order Bessel vortex beam are performed to investigate the effect of varying the half-cone angle on the 3D directivity plots. The results are shown in Fig. 4 for a size parameter $ka=5$ and for half-cone angle values ranging from $\beta=10^\circ$ to $\beta=80^\circ$ in increments of $\delta\beta=10^\circ$. The arrows in the figure denote the direction of incident waves. In this example, the rigid sphere is shifted along the x-direction by an offset of $0.1\lambda/2a$. As observed in this figure, the symmetry in the 3D acoustic scattering directivity patterns in the far-field is further broken as β increases.

Moreover, the analysis of Eqs. (3), (4) and (14) for which the order m equals zero, show that the problem reduces to the scattering by a zero-order Bessel beam [31]. In addition, when both the order m and the half-cone angle β equal zero, the problem reduces to the scattering of plane progressive waves by a sphere [6].

Another example is provided in Fig. 5 in which the order of the beam m and the size parameter ka are varied. The computations are made for a size parameter $ka=10$ and a half-cone angle $\beta=45^\circ$ for the ease of comparison between the earlier computational

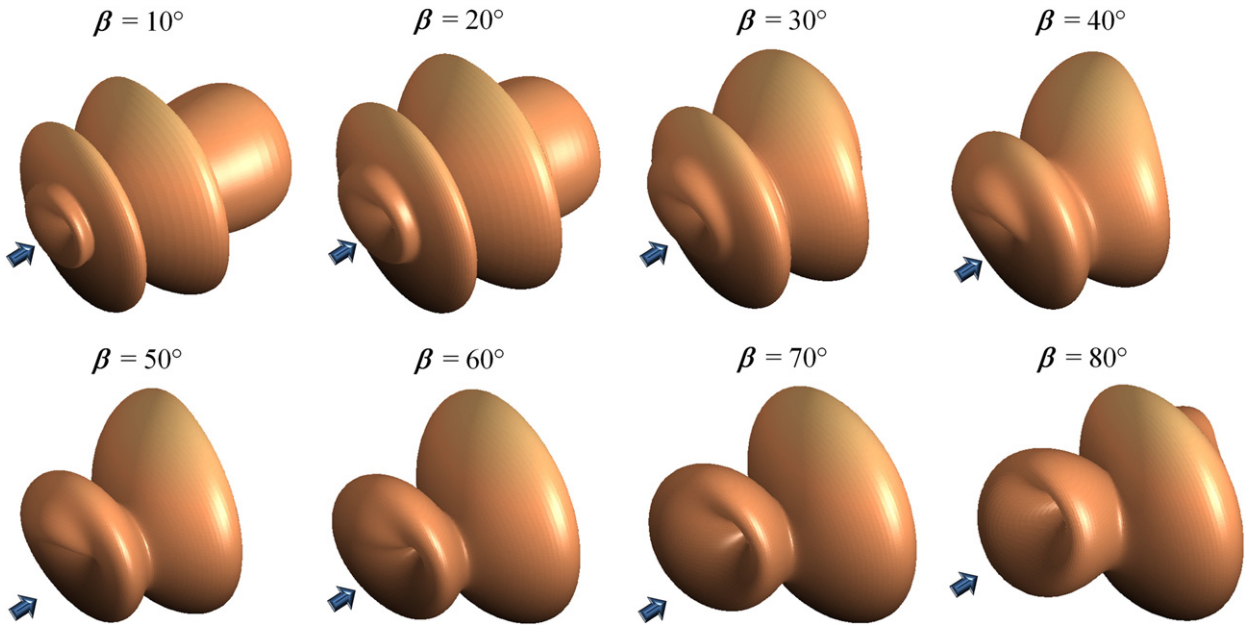

Fig. 4. The effect of varying the half-cone angle on the 3D directivity plots for the far-field acoustic scattering of a first-order Bessel vortex beam by a rigid sphere shifted along the x-direction by an offset of $0.1\lambda/2a$. The results are shown for a size parameter $ka=5$ and for half-cone angle values ranging from $\beta=10^\circ$ to $\beta=80^\circ$ in increments of $\delta\beta=10^\circ$. The arrows denote the direction of incident waves.

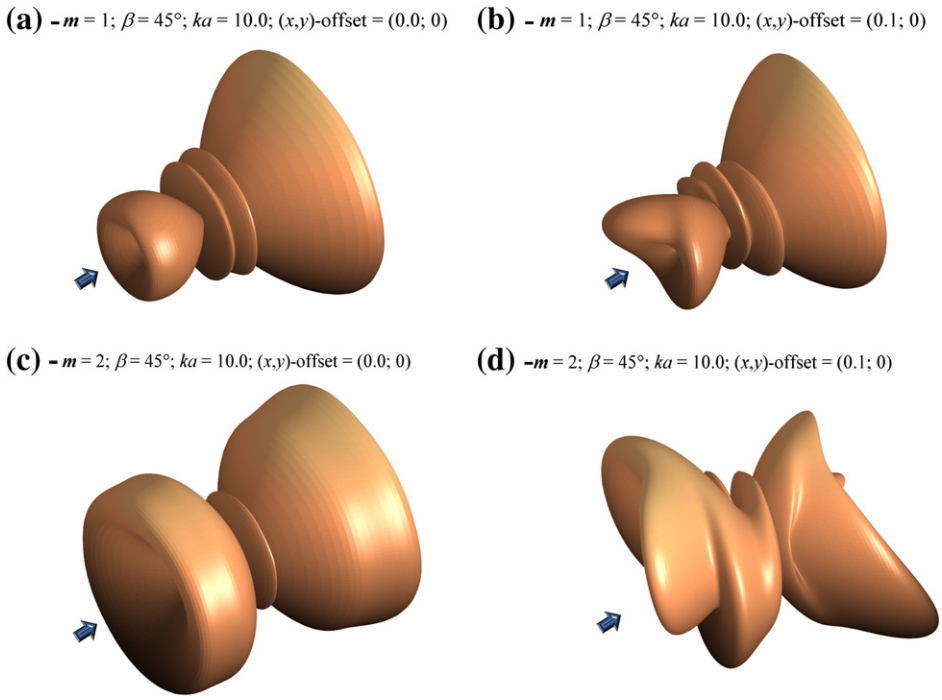

Fig. 5. The effect of varying both the order m of the high-order Bessel (vortex) beam and the size parameter ka on the 3D directivity plots of the far-field acoustic scattering. The computations are made for a size parameter $ka = 10$ and a half-cone angle $\beta = 45°$. The arrows denote the direction of the incident waves. (a),(c) correspond to the directivity patterns from a rigid sphere centered on the axis of a first- and a second-order Bessel vortex beam, respectively. Shifting the sphere *off*-axis certainly affects the scattering patterns of the higher-order Bessel vortex beams as shown in (b),(d).

plots displayed in the previous figures. The arrows in the figure denote the direction of incident waves. Fig. 5-(a),(c) corresponds to the far-field acoustic scattering directivity patterns from a rigid sphere centered on the axis of a first- and a second-order Bessel vortex beam, respectively. Shifting the sphere *off*-axis certainly affects the scattering patterns of the high-order Bessel vortex beams as shown in Fig. 5-(b),(d). As observed previously, the symmetry in the directivity plots is broken as soon as the sphere is shifted off-axis.

In all the preceding examples, the sphere is considered rigid immovable (fixed) in water. However, other types of sphere's materials can be used, provided that their appropriate scattering coefficients are used. These scattering coefficients are available in standard literature reports for elastic [6], viscoelastic spheres [32], spherical bubbles [2], soft and solid spherical shells [33,34], coated spheres [35], and coated spherical shells [36,37]. It is important to note that elastic sphere exhibit resonances that affect the acoustic scattering response. Further studies on the off-axial scattering of Bessel beams by elastic spheres are in order and will be the subject of future investigations.

It is important to emphasize here that the theory is suitable to investigate the on- and off-axial acoustic scattering for any beam that *satisfies* the homogeneous (source-free) Helmholtz wave Eq. (1). It is understood that non-diffracting beams (such as the zero-order and high-order Bessel vortex and trigonometric beams of *integer* order) are adequate solutions of the homogeneous Helmholtz equation, and their acoustic scattering properties can be satisfactorily investigated through the present theory. Nevertheless, Bessel beams with a *fractional* order [38–40], Gaussian and their derivatives (i.e. Bessel–Gaussian, Hermite–Gaussian, Laguerre–Gaussian, Ince–Gaussian, Hypergeometric–Gaussian and others) are generally diffractive and prone to spreading as they propagate in space, thus they do not satisfy the homogeneous Helmholtz Eq. (1) [41]. Therefore, the scattering for such (diffractive) beams may be analyzed through diffraction theory [42]. There exist, however, exceptions [43] in which a focused Gaussian beam may be considered as a good approximation of a non-diffracting beam as long as the beam waist radius is *larger* than a wavelength (See section IV in [28], also [44]), thus the present theory may be applicable in that limit. This approximation may also apply for the case of a fractional Bessel beam in that same limit and outside the region of diffraction where the beam's symmetry may be preserved. However, this problem is nonetheless acknowledged and further investigations are needed to verify that assumption.

As mentioned previously, the size parameter ka should be judiciously chosen so as to avoid the zeros of the spherical Bessel function of the first-kind (given in Table 1) in Eq. (7). In doing so, possible numerical indeterminacies in the computation of the beam-shape coefficients are circumvented. Moreover, at high ka values (i.e. $ka > 15$ and beyond), more sampling and discretization of the domain are needed to ensure proper convergence and hence guarantee the accuracy of the solution. With the aim of overcoming the numerical indeterminacies at the zeros of the spherical Bessel function of the first-kind and improving the computational time, other numerical models (analogous to the ones used in the scattering of electromagnetic radiation (i.e. light)

by a spherical particle [44–47]) that approximate the integral in Eq. (7) with an analytical converging function may be developed, however, they are outside the scope of the present research.

This present theory ignores dissipative and viscous effects as well as thermal damping. Therefore, the 3D directivity plots obtained here may only be directly relevant for cases where the radius of the sphere is larger than the oscillating thermo-viscous boundary layer produced by the incident wave in the vicinity of the sphere in a viscous fluid. This present analysis should assist the development of complete acoustic scattering models that include viscous effects, streaming and thermal damping that may be significant in highly viscous fluids.

4. Conclusions

In summary, theoretical expressions for the incident and scattered acoustic pressure fields are derived, and for the first time, numerical calculations of near-surface and far-field acoustic scattering directivity 3D diagrams are presented for a rigid sphere placed off the axial center of a high-order Bessel vortex beam. A quantitative analysis of the scattering on- and off-axis is provided in both near- and far-field regions for various half-cone angle values. When the sphere is placed on-axis, the backward scattering and forward scattering vanish for all frequencies as shown previously [12]. However, when the sphere is shifted off the beam's axis of wave propagation, significant modifications in the directivity plots occur, which are determined by the amount of the shift, the choices for the frequency as well as varying the beam's order and its half-cone angle. In addition to providing physical insight into the off-axial scattering of acoustic Bessel vortex beams, this investigation would potentially assist in the development of the transverse acoustic radiation force and could provide a useful test of finite element codes for the evaluation of the scattering. Furthermore, the theory developed here can be extended to study the off-axial electromagnetic scattering by dielectric [48], conductive, or other types of spheres.

Supplementary materials related to this article can be found online at doi:10.1016/j.wavemoti.2011.02.001.

Acknowledgments

Dr. Mitri acknowledges the financial support provided through a Director's fellowship (LDRD-X9N9) from Los Alamos National Laboratory. Dr. Silva acknowledges the funding from a grant CNPq 150745/2007-9 (Brazilian agency). Disclosure: this unclassified publication, with the following reference no. LA-UR 11-00970, has been approved for unlimited public release under DUSA ENSCI.

References

[1] A. Lagendijk, B.A. van Tiggelen, Resonant multiple scattering of light, Phys. Rep. 270 (1996) 143–215.
[2] L. Flax, G.C. Gaunaurd, H. Uberall, Theory of Resonance Scattering, Phys. Acoust. 15 (1981) 191–294.
[3] G.C. Gaunaurd, Elastic and acoustic resonance wave scattering, Appl. Mech. Rev. 42 (1989) 143–192.
[4] G.C. Gaunaurd, M.F. Werby, Acoustic resonance scattering by submerged elastic shells, Appl. Mech. Rev. 43 (1990) 171–208.
[5] G.C. Gaunaurd, H.S. Strifors, Transient resonance scattering and target identification, Appl. Mech. Rev. 50 (1997) 131–149.
[6] J.J. Faran, Sound scattering by solid cylinders and spheres, J. Acoust. Soc. Am. 23 (1951) 405–418.
[7] G.C. Gaunaurd, H. Uberall, Acoustics of finite beams, J. Acoust. Soc. Am. 63 (1978) 5–16.
[8] P.L. Edwards, J. Jarzynski, Scattering of focused ultrasound by spherical microparticles, J. Acoust. Soc. Am. 74 (1983) 1006–1012.
[9] J.P. Barton, N.L. Wolff, H. Zhang, C. Tarawneh, Near-field calculations for a rigid spheroid with an arbitrary incident acoustic field, J. Acoust. Soc. Am. 113 (2003) 1216–1222.
[10] D.P. Duncan, J.P. Astheimer, R.C. Waag, Scattering calculation and image reconstruction using elevation-focused beams, J. Acoust. Soc. Am. 125 (2009) 3101–3119.
[11] P.L. Marston, Scattering of a Bessel beam by a sphere, J. Acoust. Soc. Am. 121 (2007) 753–758.
[12] F.G. Mitri, Acoustic scattering of a high-order Bessel beam by an elastic sphere, Ann. Phys. 323 (2008) 2840–2850.
[13] P.L. Marston, Scattering of a Bessel beam by a sphere: II. Helicoidal case and spherical shell example, J. Acoust. Soc. Am. 124 (2008) 2905–2910.
[14] F.G. Mitri, Equivalence of expressions for the acoustic scattering of a progressive high-order Bessel beam by an elastic sphere, IEEE Trans. Ultrason. Ferroelectr. 56 (2009) 1100–1103.
[15] C. Lopez-Mariscal, J.C. Gutierrez-Vega, The generation of nondiffracting beams using inexpensive computer-generated holograms, Am. J. Phys. 75 (2007) 36–42.
[16] Z. Bouchal, J. Wagner, M. Chlup, Self-reconstruction of a distorted nondiffracting beam, Opt. Commun. 151 (1998) 207–211.
[17] K. Volke-Sepulveda, A.O. Santillan, R.R. Boullosa, Transfer of angular momentum to matter from acoustical vortices in free space, Phys. Rev. Lett. 100 (2008) 024302.
[18] K.D. Skeldon, C. Wilson, M. Edgar, M.J. Padgett, An acoustic spanner and its associated rotational Doppler shift, New J. Phys. 10 (2008).
[19] S.T. Kang, C.K. Yeh, Potential-well model in acoustic tweezers, IEEE Trans. Ultrason. Ferroelectr. 57 (2010) 1451–1459.
[20] F.G. Mitri, Potential-well model in acoustic tweezers - Comment, IEEE Trans. Ultrason. Ferroelectr. 58 (2011) 663–666.
[21] F.G. Mitri, Acoustic radiation force on a sphere in standing and quasi-standing zero-order Bessel beam tweezers, Ann. Phys. 323 (2008) 1604–1620.
[22] F.G. Mitri, Langevin acoustic radiation force of a high-order Bessel beam on a rigid sphere, IEEE Trans. Ultrason. Ferroelectr. 56 (2009) 1059–1064.
[23] F.G. Mitri, Acoustic radiation force of high-order Bessel beam standing wave tweezers on a rigid sphere, Ultrasonics 49 (2009) 794–798.
[24] F.G. Mitri, Acoustic radiation force on an air bubble and soft fluid spheres in ideal liquids: example of a high-order Bessel beam of quasi-standing waves, Eur. Phys. J. E 28 (2009) 469–478.
[25] F.G. Mitri, Negative axial radiation force on a fluid and elastic spheres illuminated by a high-order Bessel beam of progressive waves, J. Phys. A: Math. Theor. 42 (2009) 245202.
[26] P.L. Marston, Radiation force of a helicoidal Bessel beam on a sphere, J. Acoust. Soc. Am. 125 (2009) 3539–3547.
[27] F.G. Mitri, Interaction of a nondiffracting high-order Bessel (vortex) beam of fractional type α and integer order m with a rigid sphere: Linear acoustic scattering and net instantaneous axial force, IEEE Trans. Ultrason. Ferroelectr. 57 (2010) 395–404.
[28] J.P. Barton, D.R. Alexander, S.A. Schaub, Internal and near-surface electromagnetic-fields for a spherical-particle irradiated by a focused laser-beam, J. Appl. Phys. 64 (1988) 1632–1639.
[29] W.G. Neubauer, R.H. Vogt, L.R. Dragonette, Acoustic reflection from elastic spheres. I. Steady-state signals, J. Acoust. Soc. Am. 55 (1974) 1123–1129.

[30] L.R. Dragonette, R.H. Vogt, L. Flax, W.G. Neubauer, Acoustic reflection from elastic spheres and rigid spheres and spheroids. II. Transient analysis, J. Acoust. Soc. Am. 55 (1974) 1130–1137.
[31] G.T. Silva, Off-axis scattering of an ultrasound Bessel beam by a sphere, IEEE Trans. Ultrason. Ferroelectr. 58 (2011) 298–304.
[32] V.M. Ayres, G.C. Gaunaurd, Acoustic resonance scattering by viscoelastic objects, J. Acoust. Soc. Am. 81 (1987) 301–311.
[33] F.G. Mitri, Acoustic radiation force acting on elastic and viscoelastic spherical shells placed in a plane standing wave field, Ultrasonics 43 (2005) 681–691.
[34] F.G. Mitri, Acoustic radiation force acting on absorbing spherical shells, Wave Motion 43 (2005) 12–19.
[35] F.G. Mitri, Acoustic radiation force due to incident plane-progressive waves on coated spheres immersed in ideal fluids, Eur. Phys. J. B 43 (2005) 379–386.
[36] G.C. Gaunaurd, A. Kalnins, Resonances in the sonar cross sections of coated spherical shells, Int. J. Solids Struct. 18 (1982) 1083–1102.
[37] F.G. Mitri, Calculation of the acoustic radiation force on coated spherical shells in progressive and standing plane waves, Ultrasonics 44 (2006) 244–258.
[38] S.H. Tao, W.M. Lee, X.C. Yuan, Dynamic optical manipulation with a higher-order fractional Bessel beam generated from a spatial light modulator, Opt. Lett. 28 (2003) 1867–1869.
[39] S.H. Tao, W.M. Lee, X.C. Yuan, Experimental study of holographic generation of fractional Bessel beams, Appl. Opt. 43 (2004) 122–126.
[40] S.H. Tao, X.C. Yuan, Self-reconstruction property of fractional Bessel beams, J. Opt. Soc. Am. A Opt. Image Sci. Vis. 21 (2004) 1192–1197.
[41] F.G. Mitri, Gegenbauer expansion to model the incident wave-field of a high-order Bessel vortex beam in spherical coordinates, Ultrasonics 50 (2010) 541–543.
[42] J.T. Hodges, G. Gréhan, G. Gouesbet, C. Presser, Forward scattering of a Gaussian beam by a nonabsorbing sphere, Appl. Opt. 34 (1995) 2120–2132.
[43] P. Varga, P. Török, The Gaussian wave solution of Maxwell's equations and the validity of scalar wave approximation, Opt. Commun. 152 (1998) 108–118.
[44] J.A. Lock, Improved Gaussian beam-scattering algorithm, Appl. Opt. 34 (1995) 559–570.
[45] B.R. Johnson, Light scattering by a multilayer sphere, Appl. Opt. 35 (1996) 3286–3296.
[46] W. Yang, Improved recursive algorithm for light scattering by a multilayered sphere, Appl. Opt. 42 (2003) 1710–1720.
[47] http://en.wikipedia.org/wiki/Codes_for_electromagnetic_scattering_by_spheres.
[48] F.G. Mitri, Arbitrary scattering of an electromagnetic zero-order Bessel beam by a dielectric sphere, Opt. Lett. 36 (2011) 766–768.